

Josephson effect between triplet superconductors through a finite ferromagnetic barrier

B. Bujnowski,* C. Timm,† and P. M. R. Brydon‡

Institut für Theoretische Physik, Technische Universität Dresden, 01062 Dresden, Germany

(Dated: November 23, 2018)

Charge and spin transport in a junction involving two triplet superconductors and a ferromagnetic barrier are studied. We use Bogoliubov-de Gennes wavefunctions to construct the Green's function, from which we obtain the Josephson currents in terms of the Andreev reflection coefficients. We focus on the consequences of a finite barrier width for the occurrence of $0-\pi$ transitions and for the spin currents, and examine the appropriateness of the common δ -function approximation for the tunneling region.

PACS numbers: 74.50.+r, 74.20.Rp

I. INTRODUCTION

Josephson junctions between spin-singlet superconductors with ferromagnetic tunneling barriers have recently attracted much interest.¹⁻³ Since spin-singlet superconductivity is strongly suppressed by the exchange splitting of the Fermi surface in the ferromagnet, such junctions represent a unique way of probing the interplay of two competing states. A startling consequence is the so-called $0-\pi$ transition: By varying the width of the ferromagnetic tunneling barrier or changing the magnitude of the exchange splitting, the current vs. phase relationship reverses sign relative to the non-magnetic case.⁴⁻¹⁹ Roughly speaking, the pair-breaking effect of the exchange fields causes a spatial oscillation of the superconducting pairing correlations within the ferromagnetic tunneling barrier, which can therefore connect the two superconductors with either a 0 or π phase shift. This phenomenon has been the subject of intense theoretical¹⁻¹⁴ and experimental¹⁵⁻¹⁹ interest and is by now very well understood.

At least from a theoretical point of view, it is therefore surprising that the physics of triplet superconductor (TSC)–ferromagnet (FM) bilayers²⁰⁻²⁵ and junctions has received relatively little attention.^{11,22,26-32} Due to the intimate relationship between triplet pairing and ferromagnetism, one would anticipate very different behavior compared to the singlet case. Recently, several papers have pointed out that the orientation of the magnetization relative to the TSC vector order parameter is a key parameter of such systems, leading to a variety of exotic effects: A universal $0-\pi$ transition dependent upon the orientation of the magnetic moment, an intimate connection between spin and charge Josephson effects, and also phase-independent Josephson spin currents.^{23,25,29-32} Although none of these predictions have yet been verified experimentally, the recent creation of superconducting thin films of Sr_2RuO_4 is a significant step towards the fabrication of TSC-FM heterostructures.³³ A deeper understanding of the physics of these systems is therefore desirable.

Most investigations of TSC junctions were performed

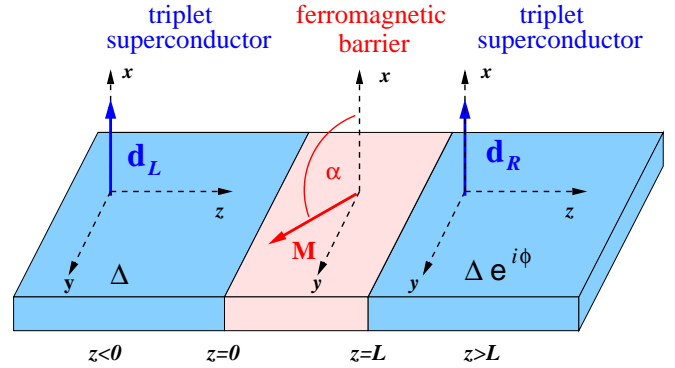


FIG. 1: Schematic diagram of the junction.

assuming an atomically thin barrier modeled by a δ -function separating the superconducting regions. The effect of a finite barrier width has only been studied by Rahnavard *et al.*³² for the case of a $(p_z + ip_y)$ -wave gap where the authors obtained results that are only partially consistent with the previous perturbative calculations³¹ for a δ -function barrier. This raises the interesting possibility that additional mechanisms for the Josephson currents appear due to the finite barrier width. It is therefore the aim of this work to systematically investigate the relationship between the results in the δ -function limit and for a more realistic barrier model. In our calculations we utilize a non-perturbative method to determine the Josephson current by solving the Bogoliubov-de Gennes (BdG) equation. We compare the results with the predictions of perturbation theory.³¹

II. THEORY

We consider a Josephson junction consisting of an FM layer of width L sandwiched between two TSCs, shown schematically in Fig. 1. The BdG equation for quasipar-

ticle states with energy E reads

$$\begin{pmatrix} \hat{\mathcal{H}}_0(\mathbf{r}) & \hat{\Delta}(\mathbf{r}) \\ \hat{\Delta}^\dagger(\mathbf{r}) & -\hat{\mathcal{H}}_0^T(\mathbf{r}) \end{pmatrix} \Psi(r) = E\Psi(r). \quad (1)$$

The noninteracting Hamiltonian is

$$\hat{\mathcal{H}}_0(\mathbf{r}) = \left[-\frac{\hbar^2}{2m} \nabla_{\mathbf{r}}^2 - \mu \right] \mathbb{1} - \Theta(z)\Theta(L-z)g\mu_B\hat{\boldsymbol{\sigma}} \cdot \mathbf{M}, \quad (2)$$

where for simplicity we assume two-dimensional circular Fermi surfaces lying in the y - z plane, as well as equal effective masses and chemical potentials in all three regions of the junction. The magnetic moment \mathbf{M} of the FM lies in the x - y plane and forms an angle α with the x axis so that

$$\mathbf{M} = M(\cos \alpha, \sin \alpha, 0). \quad (3)$$

This formulation is completely general since the TSCs are invariant under spin rotations around the x axis.

The gap matrix in equation (1) is

$$\hat{\Delta}(\mathbf{r}) = \hat{\Delta}_L\Theta(-z) + \hat{\Delta}_R\Theta(z-L), \quad (4)$$

where $\hat{\Delta}_\nu$ ($\nu = L, R$) is related to the \mathbf{d} vector by $\hat{\Delta}_\nu = i\hat{\sigma}_y(\hat{\boldsymbol{\sigma}} \cdot \mathbf{d}_\nu)$. We assume the TSCs to be in an equal-spin-pairing unitary state. In particular, we take

$$\mathbf{d}_L(\mathbf{k}) = \Delta(\mathbf{k})\mathbf{e}_x, \quad (5)$$

$$\mathbf{d}_R(\mathbf{k}) = \Delta(\mathbf{k})e^{i\phi}\mathbf{e}_x, \quad (6)$$

where $\Delta(\mathbf{k})$ denotes the orbital pairing state, so that the two superconductors differ only in the overall phase ϕ of the order parameter. In this work we will be concerned with the three orbital pairing states

$$\Delta(\mathbf{k}) = \begin{cases} \Delta(T)k_y/k_F, & p_y\text{-wave,} \\ \Delta(T)k_z/k_F, & p_z\text{-wave,} \\ \Delta(T)(k_z + ik_y)/k_F, & p_z + ip_y\text{-wave,} \end{cases} \quad (7)$$

where $\Delta(T) \cong \Delta_0\sqrt{(T_C - T)/T_C}$ is the weak-coupling temperature-dependent gap magnitude and k_F is the Fermi momentum of the normal state.

The BdG equation is solved separately in the different regions under the assumption of low-energy excitations, i.e., $\mu \gg E$, $|\Delta(\mathbf{k})|$, so that the electron and hole wavevectors can be regarded as approximately equal in magnitude, $k_e \approx k_h \approx k_F$, the so-called Andreev approximation. The dephasing of the electron and hole wavefunctions in the finite FM layer constrains the validity of this approximation to $(k_e - k_h)L \approx 2EL/\hbar v_F \ll 1$, where $v_F \approx 10^6 \text{ ms}^{-1}$ is the Fermi velocity and $E \leq \max\{|\Delta(\mathbf{k})|\} \approx 0.1 \text{ meV}$ (we assume $T_C \approx 1 \text{ K}$). This implies that we restrict ourselves to thin layers with $Lk_F \lesssim 100$. In the TSC we obtain plane-wave solutions $\psi_{\mathbf{k},e(h),\sigma} = \phi_{\mathbf{k},e(h),\sigma} e^{i\mathbf{k}\cdot\mathbf{r}}$ for electron-like (hole-like)

quasiparticles with wavevector \mathbf{k} and spin σ . The spinors are

$$\phi_{\mathbf{k},e,\uparrow} = (s_{\uparrow\mathbf{k}}u_{\mathbf{k}}, 0, v_{\mathbf{k}}, 0)^T, \quad (8)$$

$$\phi_{\mathbf{k},h,\uparrow} = (s_{\uparrow\mathbf{k}}v_{\mathbf{k}}, 0, u_{\mathbf{k}}, 0)^T, \quad (9)$$

$$\phi_{\mathbf{k},e,\downarrow} = (0, s_{\downarrow\mathbf{k}}u_{\mathbf{k}}, 0, v_{\mathbf{k}})^T, \quad (10)$$

$$\phi_{\mathbf{k},h,\downarrow} = (0, s_{\downarrow\mathbf{k}}v_{\mathbf{k}}, 0, u_{\mathbf{k}})^T, \quad (11)$$

where $u_{\mathbf{k}} = \sqrt{(E + \Omega_{\mathbf{k}})/2E}$, $v_{\mathbf{k}} = \sqrt{(E - \Omega_{\mathbf{k}})/2E}$, $\Omega_{\mathbf{k}} = \sqrt{E^2 - |\Delta(\mathbf{k})|^2}$, $s_{\sigma\mathbf{k}} = -\sigma\Delta(\mathbf{k})/|\Delta(\mathbf{k})|$, and $|\mathbf{k}| = \sqrt{2m\mu/\hbar^2} = k_F$. In the FM region we obtain plane-wave solutions $\psi_{\mathbf{k}^s,e(h),s}^{FM} = \phi_{e(h),s}^{FM} e^{i\mathbf{k}^s\cdot\mathbf{r}}$ for electron-like (hole-like) quasiparticles with wavevector \mathbf{k}^s . The spinors of spin $s = \pm$ electrons and holes are

$$\phi_{e,s}^{FM} = (se^{-i\alpha}/\sqrt{2}, 1/\sqrt{2}, 0, 0)^T, \quad (12)$$

$$\phi_{h,s}^{FM} = (0, 0, se^{i\alpha}/\sqrt{2}, 1/\sqrt{2})^T. \quad (13)$$

Due to the exchange splitting in the FM, we have majority-spin and minority-spin Fermi surfaces with radii

$$|\mathbf{k}^s| = k_F^s = \sqrt{\frac{2m}{\hbar^2}(\mu + sg\mu_B M)} = k_F\sqrt{1 + s\lambda}, \quad (14)$$

where λ denotes the ratio of the exchange splitting to the chemical potential.

We use these piecewise solutions to construct the wavefunction ansatz for a spin- σ electron-like quasiparticle incident from the left TSC with wavevector $\mathbf{k} = (k_y, k_z) = k_F(\sin\theta, \cos\theta)$, where θ is the injection angle relative to the z axis:

$$\begin{aligned} \Psi_{e,\sigma}(\mathbf{r}) = & \Theta(-z) \left\{ \psi_{\mathbf{k},e,\sigma}^L + \sum_{\sigma'=\uparrow\downarrow} [a_{\sigma\sigma'}^e \psi_{\mathbf{k},h,\sigma'}^L + b_{\sigma\sigma'}^e \psi_{-\mathbf{k},e,\sigma'}^L] \right\} \\ & + \Theta(z)\Theta(L-z) \left\{ \sum_{s=\pm} [c_{\sigma s}^e \psi_{\mathbf{k}^s,e,s}^{FM} + d_{\sigma s}^e \psi_{-\mathbf{k}^s,h,s}^{FM}] \right. \\ & \left. + e_{\sigma s}^e \psi_{-\mathbf{k}^s,e,s}^{FM} + f_{\sigma s}^e \psi_{\mathbf{k}^s,h,s}^{FM} \right\} \\ & + \Theta(z-L) \left\{ \sum_{\sigma'=\uparrow\downarrow} [g_{\sigma\sigma'}^e \psi_{\mathbf{k},e,\sigma'}^R + h_{\sigma\sigma'}^e \psi_{-\mathbf{k},h,\sigma'}^R] \right\}. \quad (15) \end{aligned}$$

A schematic representation of the wavevectors and transmission and reflection amplitudes appearing in the wavefunction $\Psi_{e,\sigma}(\mathbf{r})$ is shown in Fig. 2. For $z < 0$ this ansatz describes Andreev reflection of hole-like quasiparticles with wavevector \mathbf{k} and specular reflection of electron-like quasiparticles with wavevector $-\hat{\mathbf{k}} = (k_y, -k_z)$. These processes are weighted by their probability amplitudes $a_{\sigma\sigma'}^e$ and $b_{\sigma\sigma'}^e$, respectively. In the FM (i.e., for $0 < z < L$), the wavevectors of the transmitted and reflected quasiparticles are spin-dependent. For wavevectors of spin- s right-moving (left-moving) electrons (holes) we write $\mathbf{k}^s = (k_y, k_z^s)$, while spin- s left-moving (right-moving) electrons (holes) have wavevectors $-\tilde{\mathbf{k}}^s = (k_y, -k_z^s)$. The associated probability amplitudes for electrons (holes) are $c_{\sigma s}^e$ and $e_{\sigma s}^e$ ($d_{\sigma s}^e$ and

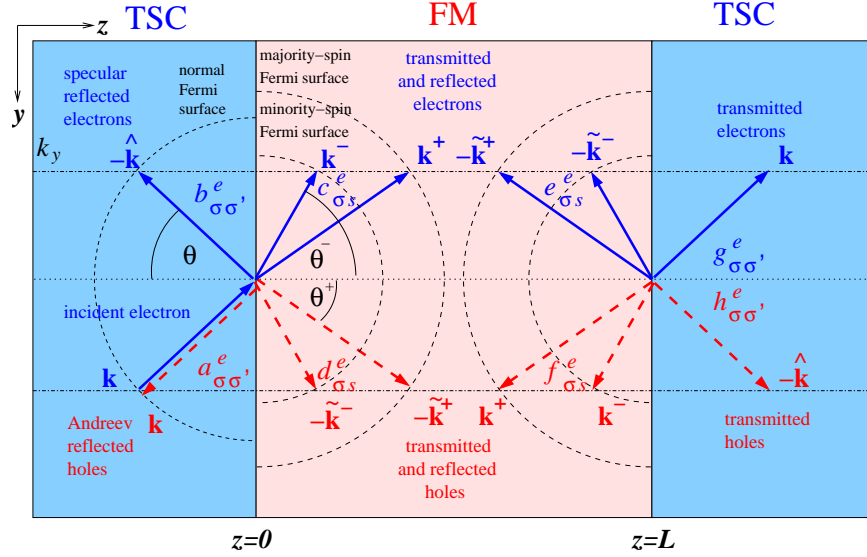


FIG. 2: (Color online) Schematic representation of the various wave vectors, amplitudes, and coefficients for a spin- σ electron-like quasiparticle incident from the left TSC, with wavefunction $\Psi_{e,\sigma}(\mathbf{r})$. The arrows denote the directions of travel of electron-like quasiparticles (solid blue) and hole-like quasiparticles (dashed red).

$f_{\sigma\sigma}^e$). For $z > L$ we have transmitted electron-like and hole-like quasiparticles with wavevectors \mathbf{k} and $-\hat{\mathbf{k}}$, and probability amplitudes $g_{\sigma\sigma'}^e$ and $h_{\sigma\sigma'}^e$, respectively. The ansatz for an incident hole-like quasiparticle $\Psi_{h,\sigma}(\mathbf{r})$ is analogous. The probability amplitudes for this case are distinguished by the superscript h , e.g., $a_{\sigma\sigma'}^h$, $b_{\sigma\sigma'}^h$ etc. Due to the translational invariance along the y axis, the wavevector component parallel to the interface is conserved during scattering, which gives

$$k_F \sin \theta = k_F^s \sin \theta^s, \quad (16)$$

where θ^s is the transmission angle for quasiparticles from the spin- s Fermi surfaces. Making use of this relation, k_z^s can be expressed as

$$k_z^s = k_F^s \cos \theta^s = k_F \sqrt{\cos^2 \theta + s\lambda}. \quad (17)$$

For injection angles

$$\theta > \theta_{\text{crit}} = \arccos \sqrt{\lambda}, \quad (18)$$

k_z^s is imaginary for minority-spin quasiparticles, i.e., the wave decays exponentially into the FM region.

The probability amplitudes for the various processes are calculated from the continuity of the wavefunction and its derivative at the interfaces,

$$\Psi_{e(h),\sigma}(\mathbf{r})|_{z=0^-} = \Psi_{e(h),\sigma}(\mathbf{r})|_{z=0^+}, \quad (19)$$

$$\Psi_{e(h),\sigma}(\mathbf{r})|_{z=L+0^-} = \Psi_{e(h),\sigma}(\mathbf{r})|_{z=L+0^+}, \quad (20)$$

$$\frac{\partial}{\partial z} \Psi_{e(h),\sigma}(\mathbf{r})|_{z=0^-} = \frac{\partial}{\partial z} \Psi_{e(h),\sigma}(\mathbf{r})|_{z=0^+}, \quad (21)$$

$$\frac{\partial}{\partial z} \Psi_{e(h),\sigma}(\mathbf{r})|_{z=L+0^-} = \frac{\partial}{\partial z} \Psi_{e(h),\sigma}(\mathbf{r})|_{z=L+0^+}. \quad (22)$$

The results for a δ -barrier can be obtained by taking the limits $L \rightarrow 0$, $\lambda \rightarrow \infty$ while keeping the product $L\lambda$ constant.

The charge current I_C and spin current I_S^μ ($\mu = x, y, z$) perpendicular to the junction interface are obtained using the Furusaki-Tsukada formulas.^{34–36} These are written in terms of the Andreev reflection coefficients $a_{\sigma\sigma'}^e$ and $a_{\sigma\sigma'}^h$, where the energy argument is analytically continued to Matsubara frequencies [$E \rightarrow i\omega_n = i(2n-1)\pi/\beta$],

$$I_C = \frac{e}{2\hbar\beta} \int dk_y \sum_{\omega_n} \sum_{\sigma} \times \left\{ \frac{|\Delta_{\mathbf{k}}|}{\Omega_{n,\mathbf{k}}} a_{\sigma\sigma}^e(\mathbf{k}, \omega_n) - \frac{|\Delta_{-\hat{\mathbf{k}}}|}{\Omega_{n,-\hat{\mathbf{k}}}} a_{\sigma\sigma}^h(-\hat{\mathbf{k}}, \omega_n) \right\}, \quad (23)$$

$$I_S^y = \frac{i}{4\beta} \int dk_y \sum_{\omega_n} \sum_{\sigma} \times \left\{ \frac{|\Delta_{\mathbf{k}}|}{\Omega_{n,\mathbf{k}}} a_{\sigma\bar{\sigma}}^e(\mathbf{k}, \omega_n) - \frac{|\Delta_{-\hat{\mathbf{k}}}|}{\Omega_{n,-\hat{\mathbf{k}}}} a_{\sigma\bar{\sigma}}^h(-\hat{\mathbf{k}}, \omega_n) \right\}, \quad (24)$$

$$I_S^z = -\frac{1}{4\beta} \int dk_y \sum_{\omega_n} \sum_{\sigma} \times \left\{ \frac{|\Delta_{\mathbf{k}}|}{\Omega_{n,\mathbf{k}}} a_{\sigma\sigma}^e(\mathbf{k}, \omega_n) - \frac{|\Delta_{-\hat{\mathbf{k}}}|}{\Omega_{n,-\hat{\mathbf{k}}}} a_{\sigma\sigma}^h(-\hat{\mathbf{k}}, \omega_n) \right\}, \quad (25)$$

where $\Omega_{n,\mathbf{k}} = \sqrt{\omega_n^2 + |\Delta_{\mathbf{k}}|^2}$, $\bar{\sigma} = -\sigma$ and $\int dk_y$ denotes the integration over all momenta parallel to the interface.³⁷ The x component of the spin current vanishes since the Cooper-pair spin is always perpendicular to the \mathbf{d} -vector.

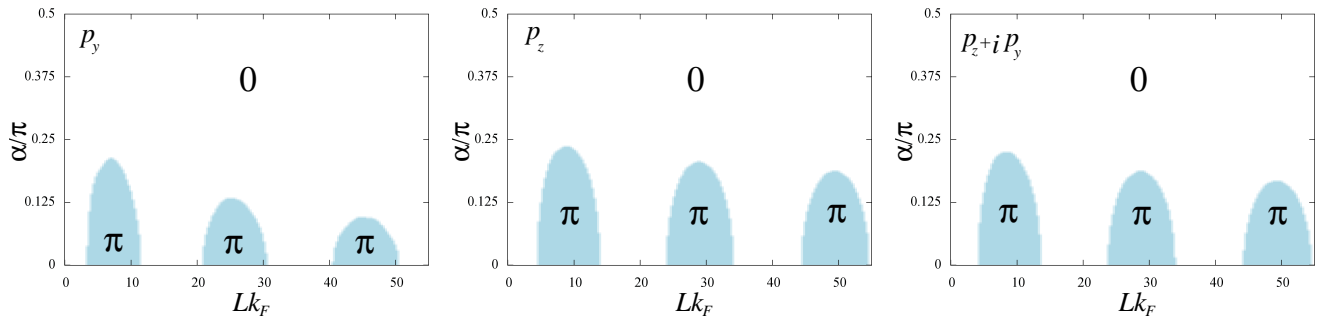


FIG. 3: Phase diagram of the junction showing 0- and π -states as a function of the angle α and barrier width L for the three considered gap symmetries. In all panels we set $T = 0.4 T_C$ and $\lambda = 0.3$.

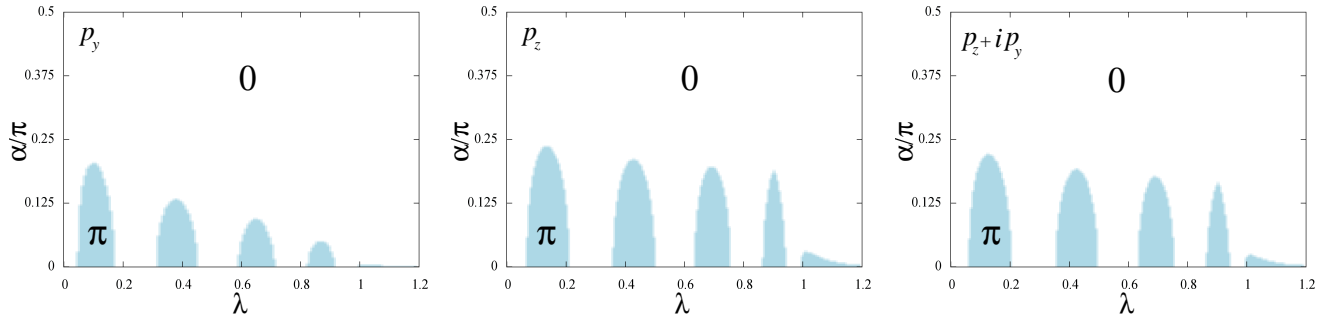


FIG. 4: Phase diagram of the junction showing 0- and π -states as a function of the angle α and exchange splitting λ for the three considered gap symmetries. In all panels we set $T = 0.4 T_C$ and $L = 20 k_F^{-1}$.

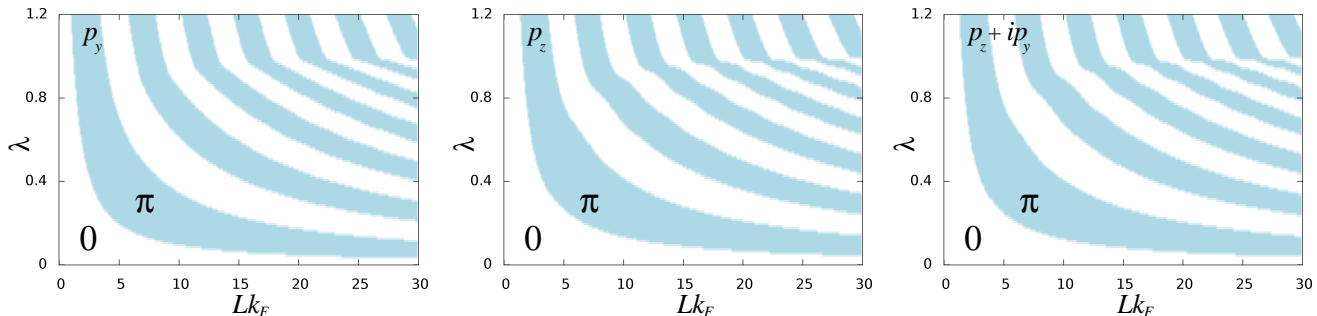


FIG. 5: Phase diagram of the junction showing 0- and π -states as a function of the exchange splitting λ and the barrier width L for the three considered gap symmetries. In all panels we set $T = 0.4 T_C$ and $\alpha = 0$.

III. RESULTS

We have numerically solved Eqs. (19)–(22) for the Andreev reflection coefficients at $T = 0.4 T_C$. At least 400 Matsubara frequencies have been used in all calculations.

A. Charge current

We are mainly interested in the occurrence of 0- π transitions, which involve a change of the phase difference ϕ of the global free-energy minimum between $\phi = 0$ and

$\phi = \pi$. Points in parameter space can be identified as corresponding to a 0-state or a π -state by examining the current-vs.-phase relationship. Specifically, we have the thermodynamic relation³⁸

$$I_C(\phi) = \frac{2e}{\hbar} \frac{\partial F}{\partial \phi} \quad (26)$$

so that $I_C = 0$ implies an extremum of the free energy F . In our system, minima only occur at $\phi = 0$ or π . We therefore numerically calculate the derivative of $I_C(\phi)$ at these two points to find out which one is a minimum. If both are minima we integrate $I_C(\phi)$ to obtain the free-

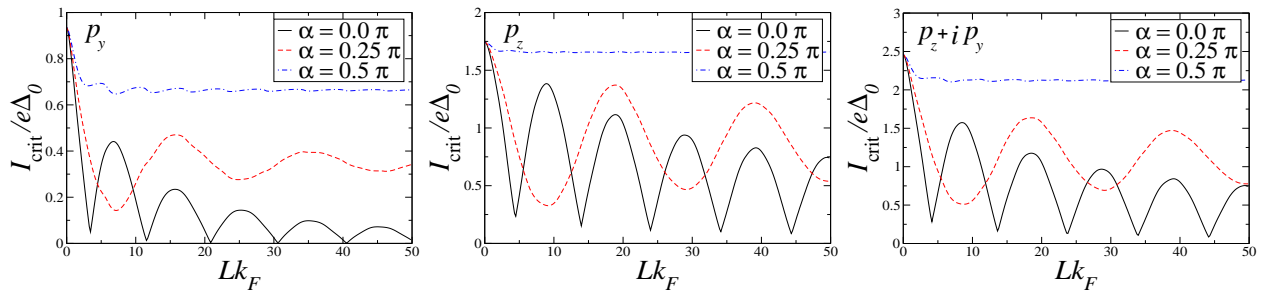


FIG. 6: Critical charge current as a function of the barrier width L . In all panels we set $T = 0.4 T_C$ and $\lambda = 0.3$.

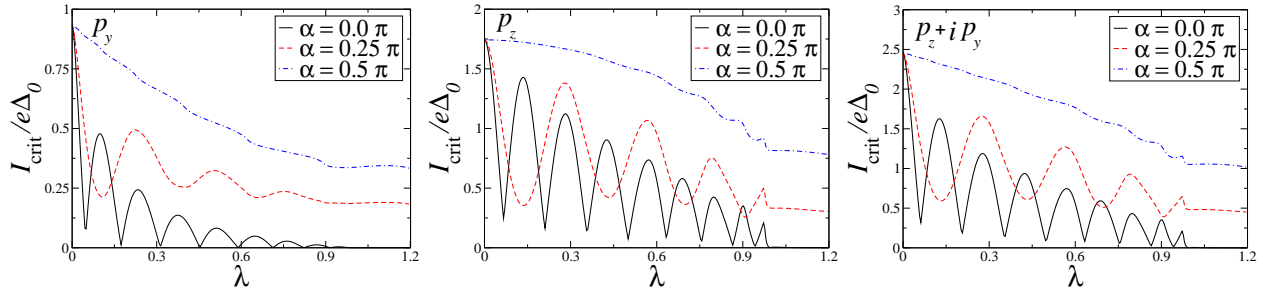


FIG. 7: Critical charge current as a function of the exchange splitting λ . In all panels we set $T = 0.4 T_C$ and $L = 20 k_F^{-1}$.

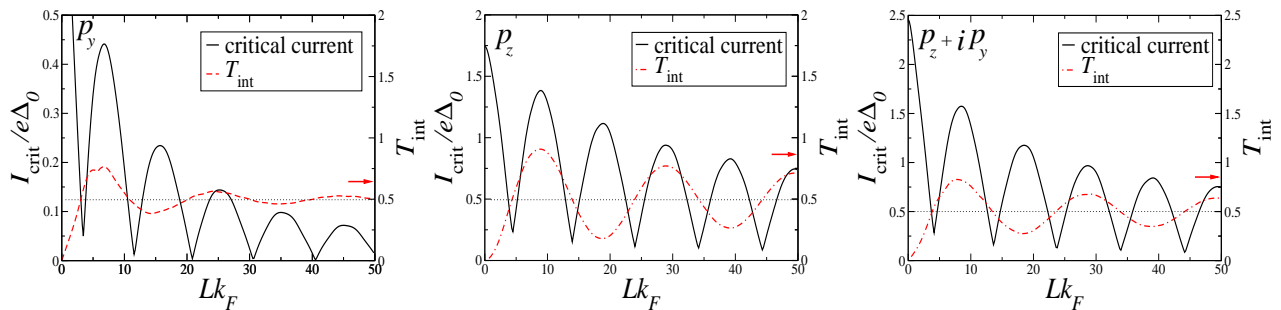


FIG. 8: Critical charge current (black solid lines, left axis) and integrated transmissivities T_{int} (red dashed lines, right axis) as functions of the barrier width L . In all panels we set $\alpha = 0$, $T = 0.4 T_C$, and $\lambda = 0.3$.

energy difference ΔF between $\phi = 0$ and π ,

$$\Delta F = \frac{\hbar}{2e} \int_0^\pi d\phi I_C(\phi), \quad (27)$$

which allows us to identify the global free-energy minimum. Using this method, we construct phase diagrams of the junction for cuts through the (α, λ, L) parameter space, which are presented in Figs. 3–5.

We find that 0 - π transitions are possible for all considered gap symmetries by increasing the magnitude of the magnetization, rotating the magnetization within the x - y plane, or by increasing the barrier width L . For $\lambda < 1$ in the (α, λ) maps and in the (α, L) maps, we find multiple dome-shaped regions where the junction is in a π -state. These π -state domes are only found for $\alpha < \pi/4$ and their appearance is shifted to lower values of α by increasing

L or λ . This effect is strongest for the p_y -wave case, while the π states are much more robust for p_z -wave and $(p_z + ip_y)$ -wave pairing. In the (α, λ) maps the π -states are strongly suppressed for $\lambda > 1$.

For $\alpha = 0$, the distribution of 0 - and π -states in Fig. 5 shows a stripe-like pattern, which does not strongly depend on the pairing symmetry of the TSC but rather upon the characteristics of the barrier. In particular, the sharp bend of the stripes at $\lambda = 1$ in all panels is a signature of the onset of half-metallicity since $|\mathbf{k}_F^-|$ vanishes at $\lambda = 1$. Interestingly, these phase diagrams are very similar to those obtained for a junction involving *singlet* superconductors on both sides of the barrier.¹⁴ The parallels between these different junctions originate from the universal pair-breaking effect of the FM-layer. Note that for the TSC case the FM layer is purely pair-

breaking only for $\alpha = 0$, and pair-breaking is completely suppressed upon increasing α to $\alpha = \pi/2$. In contrast, for a singlet-superconductor junction the FM layer is purely pair-breaking for all α . A $0-\pi$ transition caused by varying the orientation of the magnetic moment is therefore an unambiguous experimental signature of triplet superconductivity.

The direct observation of π -junctions is not trivial, as it requires the detection of half vortices at the barrier.^{16,19} A more practical experimental signature is provided by the critical charge current

$$I_{\text{crit}} = \max \{|I_C(\phi)|\}, \quad \phi \in [0, \pi]. \quad (28)$$

As the junction is tuned through a $0-\pi$ transition, the sign change of the dominant $\sin \phi$ term in the charge current $I_C(\phi)$ causes the appearance of sharp, cusp-like minima where I_{crit} nearly vanishes.⁴ If $I_C(\phi)$ were exactly proportional to $\sin \phi$, this sign change would exactly coincide both with $I_{\text{crit}} = 0$ and with a $0-\pi$ transition; the presence of weak higher harmonics in $I_C(\phi)$ complicates the analysis, but the minima in I_{crit} nevertheless remain a good proxy for the $0-\pi$ transition. We plot I_{crit} as a function of L and λ for $\alpha = 0, \pi/4$, and $\pi/2$ in Figs. 6 and 7. The sharp minima in the critical current characteristic of the $0-\pi$ transition are only found at $\alpha = 0$, and are in good agreement with the phase boundaries in Figs. 3 and 4. Upon increasing α , the sharp minima disappear by $\alpha = \pi/4$ and are replaced by broad minima in I_{crit} , which coincide with every second maximum of the $\alpha = 0$ critical current. These minima do not correspond to sign changes of the $\sin \phi$ term. At $\alpha = \pi/2$, most structure in I_{crit} has vanished.

The charge current found by perturbation theory for a δ -barrier junction is,³¹

$$I_C^{\text{pert}}(\phi) \propto (T_{\text{sp}} - T_{\text{sf}} \cos 2\alpha) \sin \phi, \quad (29)$$

where T_{sp} and T_{sf} denote the positive tunneling matrix elements for spin-preserving tunneling and spin-flip tunneling, respectively. As one can see, a π -state can only be realized if $T_{\text{sp}} < T_{\text{sf}}$ and $\alpha < \pi/4$, with the latter condition clearly consistent with the phase diagrams and critical current plots.

It is interesting to see if Eq. (29) is also valid in the finite-barrier case if we regard T_{sp} and T_{sf} as functions of L and λ . The matrix elements T_{sp} and T_{sf} are expected to be roughly proportional to the corresponding transmissivities.³¹ Note that the transmissivities are independent of α for both the δ -function and finite width barriers. From Eq. (29) we see that the spin-flip transmissivity \mathcal{T}_{sf} should be larger than the spin-preserving transmissivity \mathcal{T}_{sp} in a π -state, whereas the opposite should be true in a 0 -state. We have obtained \mathcal{T}_{sf} and \mathcal{T}_{sp} from the scattering matrix of the FM barrier, which does not change below T_C .^{7,39} As the Josephson current is expected to be proportional to the square of the TSC gap magnitude, we introduce an angular weighting of the transmissivities to account for the direction dependence

of the gap. We therefore define the integrated transmissivity

$$T_{\text{int}} = \frac{\int_{-\pi/2}^{\pi/2} d\theta \mathcal{T}_{\text{sf}} \tilde{\Delta}_\theta^2}{\int_{-\pi/2}^{\pi/2} d\theta (\mathcal{T}_{\text{sp}} + \mathcal{T}_{\text{sf}}) \tilde{\Delta}_\theta^2} \quad (30)$$

with

$$\tilde{\Delta}_\theta = \begin{cases} \sin \theta & \text{for } p_y\text{-symmetry,} \\ \cos \theta & \text{for } p_z\text{-symmetry,} \\ 1 & \text{for } p_z + ip_y\text{-symmetry.} \end{cases} \quad (31)$$

Spin-flip tunneling is dominant for $T_{\text{int}} > 0.5$, whereas for $T_{\text{int}} < 0.5$ spin-preserving tunneling is most important. As seen in Fig. 8, the barrier widths for which $T_{\text{int}} = 0.5$ are in very good agreement with the sharp minima of the critical current at $\alpha = 0$ and thus with the $0-\pi$ transitions. This shows that Eq. (29) gives a good description of the relevant physics if one includes the L - and λ -dependence of the transmissivities.

In Fig. 8 we also see that the convergence of T_{int} towards 0.5 with increasing L is much faster for p_y -symmetry compared to the other cases. Due to the p_y -wave form factor, shallow incident angles dominate the integral in Eq. (30), which implies averaging over quasi-particle trajectories corresponding to a large range of effective barrier widths. Since the probability of spin-flip transmission oscillates with the effective barrier width, increasing L rapidly leads to equal integrated probabilities of spin-flip and spin-preserving transmission. In contrast, T_{int} decreases more slowly for p_z -symmetry since the weighting favors normal incidence, and thus the average is over a smaller range of effective barrier widths. The angle-independent weighting for the $(p_z + ip_y)$ -wave case lies between these two extremes. From Eq. (29) we hence deduce that the π state in the p_y -wave junction is much less robust to increasing L than for the other cases, consistent with Fig. 3. Since increasing λ decreases the length scale of the oscillation between spin-flip and spin-preserving transmission, this argument also explains the strong suppression of the π states in the p_y -wave junction at moderate to strong polarizations in the (α, λ) maps (Fig. 4).

The loss of every second peak in the $\alpha = 0$ critical current upon increasing α to $\pi/4$ can be understood from Eq. (29) as resulting from a vanishing spin-flip contribution. As evidenced by the plots of T_{int} in Fig. (8) the relative strength of \mathcal{T}_{sf} and \mathcal{T}_{sp} oscillates with L and λ . By removing the spin-flip contribution at $\alpha = \pi/4$, the variation of the spin-preserving transmissivity on these quantities is evidenced in the critical current. Further support for this interpretation comes from the observation that every second maximum in the $\alpha = 0$ critical current also corresponds to a maximum in T_{int} , i.e., strong spin-flip tunneling and weak spin-preserving tunneling.

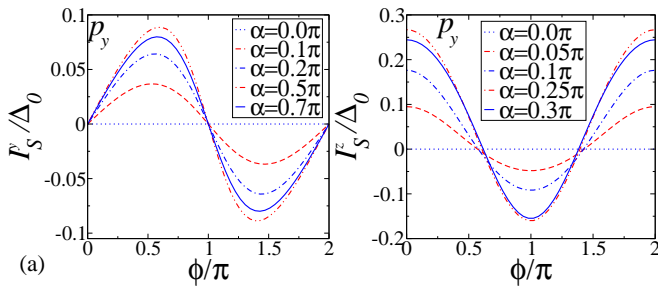


FIG. 9: Spin-current components (a) I_S^y , which is due to spin filtering, and (b) I_S^z , due to spin flip, as functions of the phase difference ϕ . In both panels we set $L = 10 k_F^{-1}$, $\lambda = 0.3$, and $T = 0.4 T_C$.

B. Spin current

We find that the polarization of the spin current always lies in the y - z plane. The y and z components are plotted in Fig. 9 for the p_y -wave case; the results are qualitatively identical for the other orbital symmetries. We show below that these two polarizations are due to different mechanisms, as proposed by Brydon *et al.*³⁰

The y component of the spin current shows the α and ϕ dependence expected for a spin-filtering mechanism.^{29,30} It occurs when the magnetic moment of the barrier has a component perpendicular to both \mathbf{d} -vectors of the TSCs. The spin- \uparrow and spin- \downarrow states with respect to this direction are not mixed by scattering at the barrier but do experience different barrier transmissivities, leading to spin filtering of the current. For a δ -function barrier, the filtering effect requires a non-magnetic scattering potential at the interface. This is not the case for a finite magnetic barrier due to the spin splitting of the Fermi surface. Specifically, minority-spin quasiparticle propagation is suppressed in the FM region above the critical injection angle θ_{crit} defined in Eq. (18), which is equivalent to a lowered transmissivity of the minority spins compared to the majority spins, giving rise to spin filtering.

The z component of the spin current shows the α and ϕ dependence expected for a spin-flipping mechanism.^{30,31} This occurs due to the spin-dependent phase shift acquired by a triplet Cooper pair when it undergoes a spin-flip during the tunneling across the barrier. This mechanism requires a component of the magnetic moment parallel to the \mathbf{d} -vectors of both TSCs. In the perturbation theory for a δ -barrier junction the z component of the spin current satisfies³¹

$$I_S^{z,\text{pert}} \propto (T_{\text{sf}} \cos \phi + \gamma R_{\text{sf}}) \sin 2\alpha, \quad (32)$$

where T_{sf} and R_{sf} are tunneling matrix elements of spin-flip tunneling and spin-flip reflection and γ is an orbital-dependent factor connected to the phase shift experienced by specularly reflected quasiparticles. For the p_y junction, there is no phase shift upon reflection and it is

found that $\gamma = 1$. In a p_z junction, reflected Cooper pairs experience a π phase shift leading to a factor of $\gamma = -1$ and in the more complicated case of a $p_z + ip_y$ junction the phase shift of the Cooper pairs depends on their incident angle as $\pi - 2 \arctan(k_y/k_z)$ so that $-1 < \gamma < 0$.

We obtain the ϕ -independent contribution $I_{S,0}^z$ by performing a Fourier transformation of $I_S^z(\phi)$. Figure 10 shows that $I_{S,0}^z$ oscillates with increasing barrier width L for all considered gap symmetries. These oscillations are due to interference between quasiparticles reflected off the two interfaces. The sign difference between $I_{S,0}^z$ for the p_y -wave and p_z -wave cases agrees with previous results;^{23,25,31} in particular, we find that the sign of the γ factor in Eq. (32) for the finite width barrier is the same as for the δ -function barrier. The $(p_z + ip_y)$ -wave case shown in Fig. 10 is intermediate between these other cases, and we find that γ can be positive or negative depending on λ and L , in contrast to the δ -function results for which the sign was found to be always negative.³¹ Specifically, in Fig. 10 we see that for $(p_z + ip_y)$ -wave symmetry $I_{S,0}^z$ is always positive at $\lambda = 0.3$, at $\lambda = 0.5$ it is negative for some values of L , and it is mostly negative at $\lambda = 0.8$.

In analogy to the procedure for the charge current, we demonstrate the appropriateness of Eq. (32) to describe the relevant physics, by showing that the oscillations of $I_{S,0}^z$ are due to oscillations of the spin-flip reflectivity \mathcal{R}_{sf} . The parameter R_{sf} in Eq. (32) is expected to be roughly proportional to the reflectivity \mathcal{R}_{sf} .³¹ Since increasing the magnetization of the barrier makes it more likely for particles to be spin-flip reflected, i.e., \mathcal{R}_{sf} should be enhanced, we see that $I_{S,0}^z$ increases with λ for all gap symmetries, see Fig. 10. We have also compared $I_{S,0}^z$ to the weighted and θ -integrated spin-flip reflectivity

$$R_{\text{int}} = \int_{-\frac{\pi}{2}}^{\frac{\pi}{2}} d\theta \mathcal{R}_{\text{sf}}(\theta) \tilde{\Delta}_\theta^2 \quad (33)$$

for a finite-barrier normal metal-FM-normal metal junction. The weighting is carried out in the same way as for the charge current except for the $p_z + ip_y$ -wave case, where it is necessary to account for the θ -dependent phase shift of quasiparticles reflected at the interface. Thus we weight the normal metal-FM-normal metal reflectivity by $\tilde{\Delta}_\theta^2 = \sin^2 \theta - \cos^2 \theta$. Fig. 11 shows that the variation of $I_{S,0}^z$ is in very good agreement with R_{int} , especially for smaller values of L and λ . We also find that the sign change in $I_{S,0}^z$ for the $(p_z + ip_y)$ -wave case reflects an important change in the nature of the spin-flip reflection:^{23,25} the positive $I_{S,0}^z$ at small λ indicates p_y -like behaviour, where tunneling of quasiparticles with high incident angles $\theta \approx \pi/2$ is dominant. At higher values of λ , however, the transmission of quasiparticles with lower incident angles $\theta \approx 0$ is favored, leading to a p_z -like behavior and hence negative $I_{S,0}^z$. We hence conclude that when the L and λ dependence of the transmissivity and reflectivity are taken into account, Eq. (32) qualitatively captures the observed behavior of the spin current.

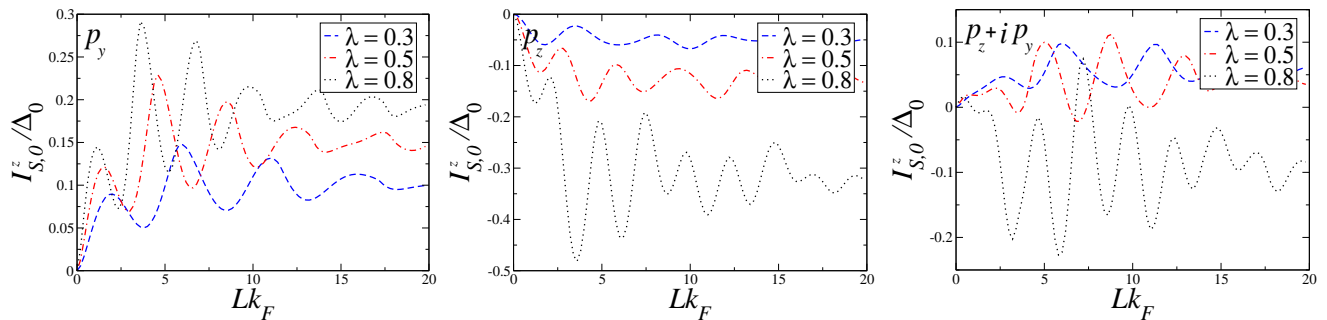


FIG. 10: ϕ -independent contributions to the spin current as functions of the barrier width L for all considered gap symmetries and various exchange splittings λ . In all panels we set $\alpha = 0.25\pi$ and $T = 0.4T_C$.

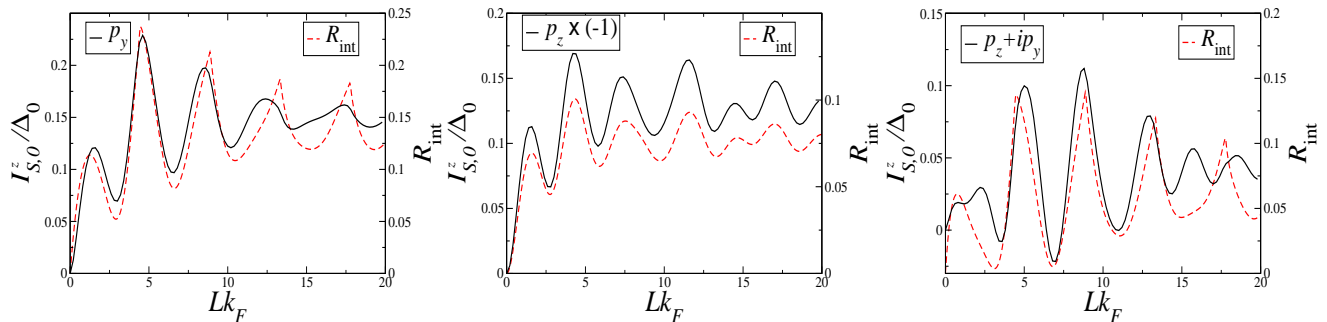


FIG. 11: ϕ -independent part of the z component of the spin current (black solid line, left axis) and integrate spin-flip reflectivity R_{int} (red dashed line, right axis) as functions of the barrier width L for all considered gap symmetries. For p_z -wave the current is multiplied by -1 for better comparability. We set $T = 0.4T_C$ and $\lambda = 0.5$ in all panels.

IV. SUMMARY AND DISCUSSION

In this paper we have studied the charge and spin currents in a TSC-FM-TSC junction. For the charge current, we have found that transitions from a 0 - to a π -state are induced by rotating the magnetization of the FM barrier in the plane parallel to the \mathbf{d} -vectors of both TSCs or by varying its magnitude. These effects have already been predicted for a δ -function barrier.³¹ In addition, we have found that changing the barrier width can also cause a 0 - π transition. In all cases, 0 - π transitions are accompanied by sharp minima of the critical current, which can thus serve as diagnostics. For the case of $(p_z + ip_y)$ -wave symmetry, our results for the critical charge current agree with Rahnavard *et al.*³² However, we have gone beyond their work by considering two additional gap symmetries, by obtaining 0 - π phase maps, and by extending the range of the exchange splitting. Furthermore, we have explained the origin of the charge current in terms of the variation of the spin-flip and spin-preserving transmissivities: for all considered gap symmetries and barrier parameters, the latter dominates over the former in a 0 -state, whereas the opposite is true for a π -state. This result is consistent with lowest-order perturbation theory.

The spin currents in the finite-barrier case can be clas-

sified in the same manner as for the δ -function barrier, i.e., we find spin currents due to spin filtering and to spin flipping. Unlike for the δ -function barrier, however, the spin-filtering effect can occur in the absence of a finite charge scattering potential because of the spin splitting of the Fermi surface in the FM barrier. For the spin current in the $(p_z + ip_y)$ -wave case we find very different polarizations and phase dependences compared to Rahnavard *et al.*³² Specifically, the authors of Ref. 32 found a spin current polarization parallel to the \mathbf{d} -vector, which is inconsistent with the fact that the spin of the Cooper pairs is always perpendicular to the \mathbf{d} -vector. The origin of this discrepancy might be that, in contrast to our work, in Ref. 32 the spin current was evaluated in the FM region, where the spin current is not a conserved quantity and is position dependent.

Overall, our results show that approximating the barrier as a δ -function gives a qualitatively correct account of the Josephson currents in a TSC-FM-TSC junction. This demonstrates the robustness and, since a metallic ferromagnetic barrier is realizable in a Josephson junction, the experimental relevance of the previously predicted phenomena.^{30,31,36} In particular, the sign reversal of the current upon varying the orientation of the magnetic moment is found to be a robust test of triplet superconductivity. The inclusion of a finite barrier width

is nevertheless crucial for a quantitatively realistic description, as the barrier width can by itself control $0-\pi$ transitions of the junction.

Acknowledgments

We have profited from discussions with G. Annunziata and T. Yokoyama.

-
- * Electronic address: bogusz.bujnowski@mailbox.tu-dresden.de
- † Electronic address: carsten.timm@tu-dresden.de
- ‡ Electronic address: brydon@theory.phy.tu-dresden.de
- ¹ A. A. Golubov, M. Y. Kupriyanov, and E. Il'ichev, *Rev. Mod. Phys.* **76**, 411 (2004).
 - ² A. I. Buzdin, *Rev. Mod. Phys.* **77**, 935 (2005).
 - ³ F. S. Bergert, A. F. Volkov, and K. B. Efetov, *Rev. Mod. Phys.* **77**, 1321 (2005).
 - ⁴ A. I. Buzdin, L. N. Bulaevskii, and S. V. Panyukov, *Sov. Phys. JETP Lett.* **35**, 178 (1981).
 - ⁵ A. V. Andreev, A. I. Buzdin, and R. M. Osgood, *Phys. Rev. B* **43**, 10124 (1991).
 - ⁶ Y. Tanaka and S. Kashiwaya, *Physica C* **274**, 357 (1997).
 - ⁷ M. Fogelström, *Phys. Rev. B* **62**, 11812 (2000).
 - ⁸ M. Eschrig, J. Kopu, J. C. Cuevas, and G. Schön, *Phys. Rev. Lett.* **90**, 137003 (2003).
 - ⁹ Z. Radović, N. Lazarides, and N. Flytzannis, *Phys. Rev. B* **68**, 014501 (2003).
 - ¹⁰ Y. Asano, Y. Tanaka, and A. A. Golubov, *Phys. Rev. Lett.* **98**, 107002 (2007).
 - ¹¹ T. Yokoyama, Y. Tanaka, and A. A. Golubov, *Phys. Rev. B* **76**, 094514 (2007).
 - ¹² M. Eschrig and T. Löfwander, *Nature Physics* **4**, 138 (2008).
 - ¹³ R. Grein, M. Eschrig, G. Metalidis, and G. Schön, *Phys. Rev. Lett.* **102**, 227005 (2009).
 - ¹⁴ G. Annunziata, H. Enoksen, J. Linder, M. Cuoco, C. Noce and A. Sudbø, *Phys. Rev. B* **83**, 144520 (2011).
 - ¹⁵ V. V. Ryazanov, V. A. Oboznov, A. Y. Rusanov, A. V. Veretennikov, A. A. Golubov, and J. Aarts, *Phys. Rev. Lett.* **86**, 2427 (2001).
 - ¹⁶ E. Goldobin, A. Sterck, T. Gaber, D. Koelle, and R. Kleiner, *Phys. Rev. Lett.* **92**, 057005 (2004).
 - ¹⁷ M. Weides, M. Kemmler, H. Kohlstedt, R. Waser, D. Koelle, R. Kleiner, and E. Goldobin, *Phys. Rev. Lett.* **97**, 247001 (2006).
 - ¹⁸ R. S. Keizer, S. T. B. Gonennenwein, T. M. Klapwijk, G. X. Miao, G. Xiao, and A. Gupta, *Nature* **439**, 825 (2006).
 - ¹⁹ J. Pfeiffer, M. Kemmler, D. Koelle, R. Kleiner, E. Goldobin, M. Weides, A. K. Feofanov, J. Lisenfeld, and A. V. Ustinov, *Phys. Rev. B* **77**, 214506 (2008).
 - ²⁰ T. Hirai, Y. Tanaka, N. Yoshida, Y. Asano, J. Inoue, and S. Kashiwaya, *Phys. Rev. B* **67**, 174501 (2003).
 - ²¹ T. Yokoyama, Y. Tanaka, and A. A. Golubov, *Phys. Rev. B* **75**, 134510 (2007).
 - ²² K. Kuboki and H. Takahashi, *Phys. Rev. B* **70**, 214524 (2004).
 - ²³ P. M. R. Brydon, *Phys. Rev. B* **80**, 224520 (2009).
 - ²⁴ G. Annunziata, M. Cuoco, C. Noce, A. Sudbø, and J. Linder, *Phys. Rev. B* **83**, 060508(R) (2011).
 - ²⁵ P. M. R. Brydon, Y. Asano, and C. Timm, *Phys. Rev. B* **83**, 180504(R) (2011).
 - ²⁶ B. Kastening, D. K. Morr, D. Manske, and K. Bennemann, *Phys. Rev. Lett.* **96**, 047009 (2006).
 - ²⁷ Y. Sawa, T. Yokoyama, Y. Tanaka, and A. A. Golubov, *Phys. Rev. B* **75**, 134508 (2007).
 - ²⁸ Y. Sawa, T. Yokoyama, Y. Tanaka, and A. A. Golubov, *J. Low Temp. Phys.* **148**, 881 (2007).
 - ²⁹ P. M. R. Brydon, B. Kastening, D. K. Morr, and D. Manske, *Phys. Rev. B* **77**, 104504 (2008).
 - ³⁰ P. M. R. Brydon, D. Manske, and M. Sigrist, *J. Phys. Soc. Jpn.* **77**, 103714 (2008).
 - ³¹ P. M. R. Brydon and D. Manske, *Phys. Rev. Lett.* **103**, 147001 (2009).
 - ³² Y. Rahnavard, G. Rashedi, and T. Yokoyama, *J. Phys.: Condens. Matter* **23**, 275702 (2011).
 - ³³ Y. Krockenberger, M. Uchida, K. S. Takahashi, M. Nakamura, M. Kawasaki, and Y. Tokura, *Appl. Phys. Lett.* **97**, 082502 (2010).
 - ³⁴ A. Furusaki and M. Tsukada, *Solid State Commun.* **78**, 299 (1991).
 - ³⁵ S. Kashiwaya and Y. Tanaka, *Rep. Prog. Phys.* **63**, 1641 (2000).
 - ³⁶ Y. Asano, *Phys. Rev. B* **72**, 092508 (2006); *ibid.* **74**, 220501 (2006).
 - ³⁷ Note that we have corrected an error in the overall sign of $I_{\xi}^z(\phi)$ that was present in Refs. 23,31.
 - ³⁸ M. Tinkham, *Introduction to Superconductivity* (Dover Publications, New York, 1996).
 - ³⁹ M. Eschrig, C. Iniotakis, and Y. Tanaka, arXiv:1001.2486 (unpublished).